A&A 366, 241–253 (2001)
DOI: 10.1051/0004-6361:20000212
© ESO 2001

Astronomy & Astrophysics

Infrared spectral classification of OB stars with ISO-SWS

P. A. Zaal[1], A. de Koter[1], and L. B. F. M. Waters[1,2]

[1] Astronomical Institute Anton Pannekoek, University of Amsterdam, Kruislaan 403, 1098 SJ Amsterdam, The Netherlands
[2] Instituut voor Sterrenkunde, Katholieke Universiteit Leuven, Celestijnenlaan 200 B, 3001 Heverlee, Belgium

Received 4 November 1999 / Accepted 6 November 2000

Abstract. We present observations of the Brα, Brβ and Pfα lines of 16 dwarf and (sub)giant stars in the spectral range O9–B3. The observations were done using the Short Wavelength Spectrometer on board the Infrared Space Observatory, and have a signal-to-noise of $\sim$20 to >150 and a resolving power varying from $\sim$1400 to 2100. We compare the equivalent widths of these lines with predictions using non-LTE model atmospheres to investigate to what extent these infrared lines can be used to derive effective temperatures. We find that Pfα is a sensitive $T_{\rm eff}$ diagnostic for the range of spectral types investigated, and Brα for types O9–B2, yielding agreement with optical results to within 1−4 kK or one-three spectral sub-types. We find evidence for a gradient in the turbulent velocity, increasing from $\lesssim 5$ km s^{-1} for the atmospheric region in which Brα is formed to $\sim$15 km s^{-1} for the regime where Pfα originates. When this gradient in turbulent velocity is taken into account, the accuracy of the spectral type calibration is improved to $\sim$1 kK or one spectral sub-type. The gravity dependence of the strengths of the investigated infrared lines is relatively weak, and could not be used to constrain luminosity class. This failure is in part a result of the modest S/N and resolution and in part a result of a cancelation of gravity effects in the line core and line wing. Our line predictions show that He I λ 2.058 is relatively unsuited for spectral classification of O9–B3 stars. Huα, however, is expected to be an even better diagnostic as are Pfα and Brα. This line may be observed with the VLT Imager and Spectrometer for mid InfraRed when it is installed on the Very Large Telescope.

Key words. line: formation – radiative transfer – stars: atmospheres – stars: early-type – stars: fundamental parameters – infrared: stars

1. Introduction

In the study of early-type stars, the infrared (IR) spectral range is of special importance as it allows one to observe stars in regions of high optical and ultraviolet extinction. In this way one may probe, for instance, ultra compact H II as well as larger star forming regions shrouded in dust. The relative ease with which infrared light passes through dusty regions makes this spectral regime a pivotal diagnostic when investigating the formation of massive stars. Clearly, an important step in this field of research is to establish which stellar properties may be derived from spectral analysis of IR lines and to provide a spectral class calibration based on IR diagnostics only. In this paper, we address aspects of this spectral class calibration focussing on stars of spectral type O9 through B3 and luminosity class V through III.

In addition to the above mentioned broad perspective, the infrared offers an unique opportunity to study an important part of the atmosphere of these early-type stars, namely that of the outer photosphere. Due to the increasing importance of free-free processes towards longer wavelengths, the prominent infrared lines are formed in different regions of the outer photosphere. This allows one to study possible gradients in atmospheric properties, such as in the amount of (micro)turbulence, in this regime.

In this paper, we will study the behaviour of a number of IR lines observed in 16 stars using the Short Wavelength Spectrometer (SWS, de Graauw et al. 1996) on board the Infrared Space Observatory (ISO, Kessler et al. 1996). The SWS covers the wavelength range from 2.4 to 45 μm. The principal goal is to investigate to what extent the Brα λ 4.05 (wavelength given in micron), Brβ λ 2.63, Pfα λ 7.46 and Pfβ λ 4.65 lines may be used for spectral type calibration. This requires one to establish which processes are relevant and, therefore, which physics needs to be included in the model calculations providing this calibration.

In O9 through B0.5 stars, Brα and Pfα are typically observed to be in emission. A grid of non-LTE plane-parallel hydrostatic models calculated in the

Send offprint requests to: A. de Koter,
e-mail: dekoter@astro.uva.nl

Table 1. The programme stars. Given are the name, HR number, HD number, spectral type, $v\sin i$ and visual magnitude. The spectral types are from Walborn (1972, 1973) in case of the O-type stars. The spectral types of the B stars, $v\sin i$ and m_V are taken from the Bright Star Catalogue and its supplement (Hoffleit & Jaschek 1982; Hoffleit et al. 1983). An asterisk in the first column indicates the star shows or has shown pulsations. δ Sco has been identified as a Be star by Coté & van Kerkwijk (1993). Therefore, the assigned spectral type for this star differs from that in the Bright Star Catalogue

name	HR	HD	Spt.	$v\sin i$ km s^{-1}	m_V mag
δ Cir	5664	135240	O7.5III(f)	189	5.09
10 Lac*	8622	214680	O9V	31	4.88
τ Sco	6165	149438	B0V	24	2.82
θ Car	4199	93030	B0Vp	151	2.76
δ Sco*	5953	143275	B0.3 IVe	181	2.32
β Cru*	4853	111123	B0.5 III	38	1.25
α Cru	4730	108248	B0.5 IV	117	1.33
α Vir*	5056	116658	B1 III-IV +B2V	159	0.98
β Cen*	5267	122451	B1 III	139	1.25
ϵ Cen*	5132	118716	B1III	159	2.30
α Lup*	5469	129056	B1.5III/Vn	24	2.30
κ Sco*	6580	160578	B1.5III	131	2.41
γ Peg*	0039	886	B2IV	3	2.83
α Pav	7790	193924	B2IV	39	1.94
ζ Dra	6396	155763	B6III	31	3.17
β Lib	5685	135742	B8V	230	2.61

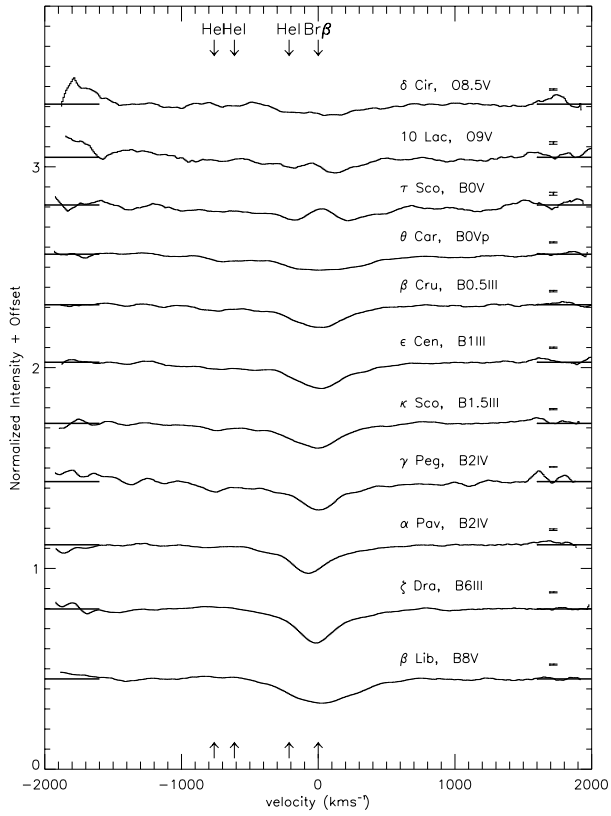

Fig. 1. Normalized Brβ spectra ordered according to spectral type. Indicated are the H I and He I lines detected in at least one of the spectra. The thick horizontal lines at the outer edges of the spectral region represent the normalization level. The errorbar on the right indicates the noise per bin in the central part of the spectrum. The edges of the spectra show higher noise values, as these parts are not scanned by all detectors

spectral analysis study of the B0 V star τ Sco (Zaal et al. 1999; hereafter Paper I), shows that such profiles are expected and result from non-LTE effects in the line forming region. In B-type stars, already small departures from LTE are amplified by stimulated emission (Sigut & Lester 1996) facilitating infrared lines to go into emission (Paper I). Murdoch et al. (1994) also sought to explain the Brα and Brγ line emission in 10 Lac (O9 V) and τ Sco by means of this non-LTE effect.

In this study, we will compare the grid of models from Paper I with the ISO spectra of our programme stars, in this way deriving effective temperatures based on infrared diagnostics alone. Although the models in this grid are relatively standard, i.e. they account for hydrogen and helium only and assume plane-parallel layers and hydrostatic equilibrium, they already show very promising results in reproducing the line strengths of Brα, Brβ and Pfα. We further investigate these results by addressing the presence of turbulent velocity fields; the possible effect of the onset of a stellar wind, and the effects of metal line blanketing on the structure of the atmosphere.

The paper is organized in the following way: the observations are described in Sect. 2. In Sect. 3, we compare observed and predicted line strengths using standard non-LTE model atmospheres. The influence of turbulence, a stellar wind and line blanketing is investigated in Sect. 4. In Sect. 5, we compare the diagnostic value of Brα and Pfα lines with other infrared diagnostics, especially with classifications using H- or K-band spectroscopy. Finally, Sect. 6 gives a summary of the main results.

2. The observations

Using the SWS instrument on board the Infrared Space Observatory we observed the Brα (4.0522 μm), Brβ (2.6259 μm), Pfα (7.4599 μm) and Pfβ (4.6538 μm) lines of 16 stars (given in Table 1). The spectra were obtained using the AOT02 grating spectral line scan mode. The spectral resolution is dependent on the wavelength and ranges from $\sim$1400 to 2100. The aperture size is $14'' \times 20''$. The programme stars were selected on (i) having a spectral type between late-O and early-B and (ii) on visual brightness and visibility during the ISO mission. The sample also includes two stars of later spectral type: ζ Dra (B6III) and β Lib (B8V). The luminosity class varies between III and V and $v\sin i$ ranges up to 220 km s^{-1}. Table 1 shows that 9 out of the 16 program stars are known to show or have shown radial pulsations. All these 9 stars are confirmed β Cephei stars, except 10 Lac and α Vir. These two are known to show (or have shown) non-radial pulsations (Smith 1978, 1985).

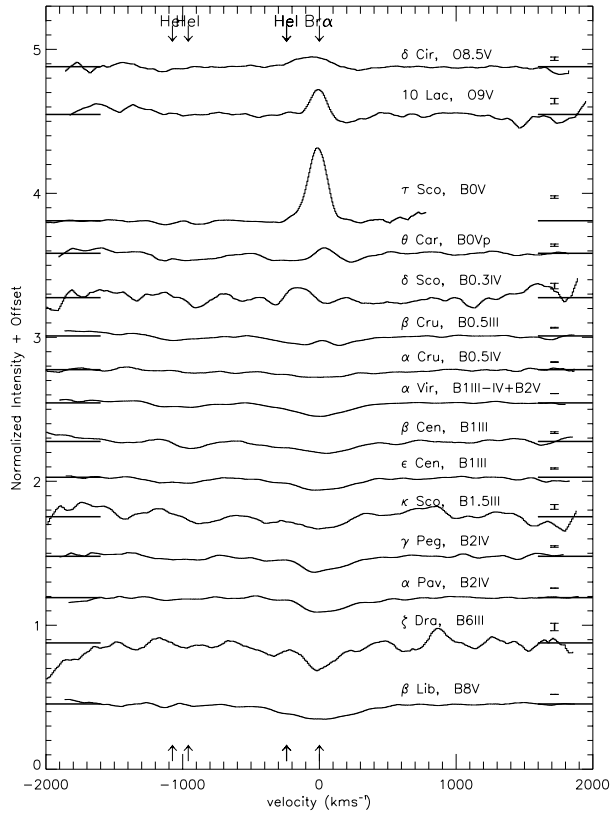

Fig. 2. Normalized Brα spectra ordered according to spectral type. Indicated are the H I and He I lines detected in at least one of the spectra. The errorbars are defined as in Fig. 1

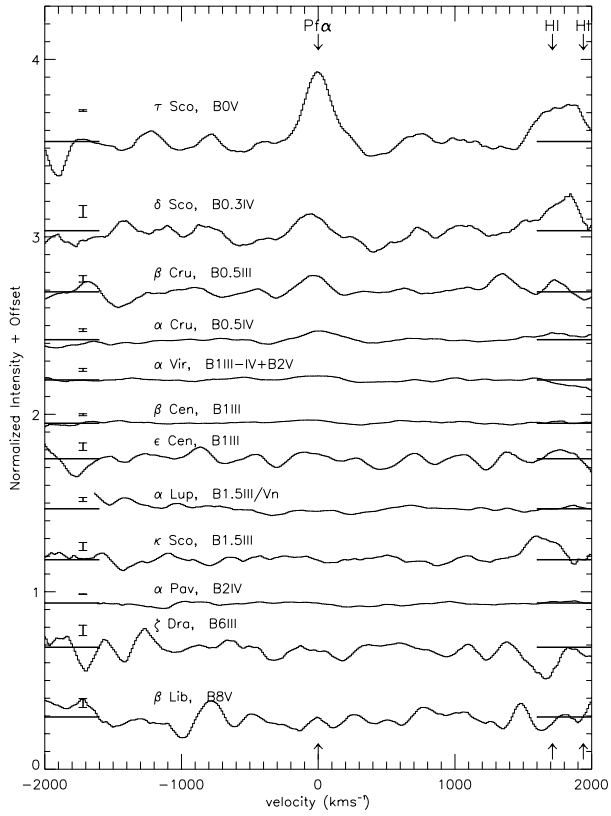

Fig. 3. Normalized Pfα spectra ordered according to spectral type. Indicated are the H I lines detected in at least one of the spectra. The errorbars are defined as in Fig. 1

The spectra were reduced using the SWS Interactive Analysis (IA^3) programs. For the data reduction we made use of the algorithms developed by Valentijn & Thi (2000). A short summary of the data reduction method is given in Paper I. We optimized the signal-to-noise (S/N) ratio of the spectra using the interactive tool "`LOW_SIGNAL`", as described by Lahuis et al. (1998). The SWS spectra suffered from fringing. The spectra were de-fringed using the fourier-filtering method in cases where the fringe was clearly present as a sharp peak in the fourier domain. Unfortunately, the Pfβ line observations were of insufficient S/N to be used in our analysis, and we discard these data in the remainder of this study. Brα is observed for all programme stars. For the other lines we note that the dataset is not homogeneous, i.e. not all lines have been observed for all stars. For instance, the Pfα profile in the late O-type stars has not been observed as these stars are relatively more distant and consequently have too low fluxes to obtain sufficient S/N. Figures 1–3 show Brβ, Brα and Pfα spectra respectively, arranged in order of progressively later spectral type. The observed line parameters for both the H I and the strongest He I lines are given in Table 2. The errorbar given in the figures represents the mean of the noise per bin in the central part of the spectrum. As the spectra are obtained in scanning mode the outer edges of the spectra show significantly lower S/N ratios compared to the central part of the scan. Only at Pfα, several of the continua show fluctuations larger than the given noise level. We attribute these fluctuations to fringes which, because of insufficient S/N, could not be filtered out.

Using the ISO Spectral Analysis Package (ISAP), we measured the line strength and width for all detected hydrogen and helium lines. The results are presented in Table 2. The listed profile parameters follow from multiple Gaussian fits to all identified line profiles within the observed spectral range. We distinguished the line absorption from the line emission in case both are clearly present. The derived line fluxes and equivalent widths for Brβ are lower limits, as the continuum is difficult to determine for this broad absorption line, especially for the late O- and earliest B-type stars (see Fig. 1).

2.1. Description of observed spectra

All three hydrogen lines show a decrease in line core emission going from early to late spectral types, where at some point the core reverts to absorption. The line emission is strongest for Pfα and Brα for which emission is detected down to spectral type B1 and B0 respectively. For Brβ weak central emission is only found in the late O-type stars and in τ Sco. The line core emission is not fully resolved

Table 2. Quantitative measurements for the observed Brβ, Brα and Pfα line spectra. Also included are other identified lines (as labeled in Table 3). For each star, the table gives for each line whether it is in absorption (a) or in emission (e); its equivalent width (EW); line flux, defined negative for absorption lines; $FWHM$; the velocity of the central absorption or emission and the line over continuum ratio at this velocity. The last column gives the S/N for the central part of the spectrum

Name	Line		EW [Å]	$F_{\rm line}$ [10^{-20} W cm^{-2}]	$FWHM$ [km s^{-1}]	$v_{\rm line}$ [km s^{-1}]	$F_{\rm l}/F_{\rm c}$	S/N
δ Cir	Brβ	(a)	–	–	–	–	–	150
	Brα	(e)	−3.0	0.9	290	−65	1.07	40
	Brα	(a)	0.6	−0.2	200	270	0.98	
	Pfα				Not detected			
10 Lac	Brβ	(e)	−0.6	0.2	145	−55	1.04	80
	Brα	(e)	−3.5	0.9	135	−5	1.18	25
	Brα	(a)	1.8	−0.5	230	195	0.94	
	Pfα				Not detected			
τ Sco	Brβ	(e)	−0.7	5.4	145	20	1.05	
	Brβ	(a)	4.3	−57	1220	10	0.96	70
	Brα	(e)	−12	17.9	155	−10	1.50	60
	Brα	(a)	7.7	−11.6	1700	–	0.97	
	He I^{d}	(a)	0.7	−1.0	150	0	0.97	
	Pfα	(e)	−23	3.0	220	0	1.39	110
	H I^{h,i}	(e)	−17	2.2	345	–	1.20	
θ Car	Brβ	(a)	4.1	−36	640	30	0.93	>150
	He I^{a,b}	(a)	0.6	−4.9	255	–	0.98	
	Brα	(e)	−3.7	5.9	205	25	1.12	60
	Brα	(a)	8.3	−13	575	−15	0.90	
	He I^{d,e}	(a)	4.7	−7.6	500	–	0.93	
	Pfα				Not detected			
δ Sco	Brβ				Not observed			
	Brα				Irregular			25
	Pfα	(e)	−5.6	1.4	185	−60	1.11	15
β Cru	Brβ	(a)	5.2	−170	510	0	0.89	135
	He I^{a,b}	(a)	1.1	−36	450	–	0.97	
	Brα	(e)	−0.6	4.0	117	15	1.04	>150
	Brα	(a)	7.7	−48	660	−15	0.92	
	He I^{d,e}	(a)	4.0	−25	570	–	0.95	
	Pfα	(e)	−4.7	2.0	185	−35	1.10	30
	H I^{h,i}	(e)	−4.4	1.9	175	–	1.09	
α Cru	Brβ				Not observed			
	Brα	(a)	6.1	−1.1	875	15	0.95	>150
	He I^{d,e}	(a)	1.1	−0.2	400	–	0.98	
	Pfα	(e)	−3.9	2.8	265	10	1.06	65
α Vir	Brβ				Not observed			
	Brα	(a)	7.1	−56	525	−15	0.91	>150
	He I^{d,e}	(a)	2.7	−22	465	–	0.96	
	Pfα	(e)	−1.8	1.1	270	−25	1.02	60
β Cen	Brβ				Not observed			
	Brα	(a)	8.0	−1.5	690	−10	0.92	80
	He I^{e}	(a)	2.1	−0.4	240	–	0.94	
	Pfα	(e)	−1.4	1.2	290	−100	1.02	90

and one should realize that in high resolution spectra core emission is typically present in Brα and Pfα down to spectral type B3. For example, Zaal et al. (1997) showed that high resolution UKIRT Brα spectra of two slowly rotating stars, ι Her (B3IV) and θ Oph (B2IV) still show weak core emission. Considering the detected trends in line emission it is clear from Figs. 2 and 3 that the Brα and Pfα emission observed for τ Sco is exceptionally strong. In Paper I, we suggest the strong H I emission in this star to be caused by large turbulent velocities in the outer photosphere, up to 150 km s^{-1}. The origin of such turbulence is not well understood, but in view of the large velocities may be connected to shocks. As non-LTE effects are expected to be enhanced by such turbulence (e.g. Sigut & Lester 1996), we expect this to be a plausible explanation for the observed strong emission. We note that large turbulent

Table 2. continued

Name	Line		EW [Å]	$F_{\rm line}$ [10^{-20} W cm^{-2}]	$FWHM$ [km s^{-1}]	$v_{\rm line}$ [km s^{-1}]	$F_{\rm l}/F_{\rm c}$	S/N
α Cru	Brβ				Not observed			
	Brα	(a)	6.1	−1.1	875	15	0.95	>150
	He I^{d,e}	(a)	1.1	−0.2	400	–	0.98	
	Pfα	(e)	−3.9	2.8	265	10	1.06	65
α Vir	Brβ				Not observed			
	Brα	(a)	7.1	−56	525	−15	0.91	>150
	He I^{d,e}	(a)	2.7	−22	465	–	0.96	
	Pfα	(e)	−1.8	1.1	270	−25	1.02	60
β Cen	Brβ				Not observed			
	Brα	(a)	8.0	−1.5	690	−10	0.92	80
	He I^{e}	(a)	2.1	−0.4	240	–	0.94	
	Pfα	(e)	−1.4	1.2	290	−100	1.02	90
ϵ Cen	Brβ	(a)	5.9	−78	520	20	0.88	>150
	He I^{a,b}	(a)	1.6	−22	540	–	0.97	
	Brα	(a)	6.9	−16	545	−15	0.91	115
	He I^{f,g}	(e)	−0.4	0.9	140	–	1.02	
	He I^{d,e}	(a)	2.4	−5.7	400	–	0.96	
	Pfα				Not suff. S/N			20
α Lup	Brβ				Not observed			
	Brα				Not observed			
	Pfα		–	–	–	–	–	45
κ Sco	Brβ	(a)	5.1	−61	475	−20	0.89	>150
	He I^{a}	(a)	1.1	−14	455	–	0.97	
	Brα				Not suff. S/N			30
	Pfα				Flat			20
γ Peg	Brβ	(a)	3.9	−29	385	−10	0.89	>150
	He I^{a}	(a)	0.8	−6.3	265	–	0.97	
	Brα	(a)	9.8	−14	575	−65	0.88	90
	He I^{f}	(e)	−1.6	2.4	195	+20	1.06	
	He I^{d,e}	(a)	1.9	−2.8	370	–	0.96	
	Pfα				Not suff. S/N			
α Pav	Brβ	(a)	5.2	−100	450	−65	0.88	125
	Brα	(a)	6.5	−26	465	40	0.90	>150
	He I^{f}	(e)	−0.5	1.9	125	25	1.03	
	He I^{d,e}	(a)	0.4	−1.4	185	–	0.99	
	Pfα				Flat			>150
ζ Dra	Brβ	(a)	6.4	−58	450	−5	0.85	>150
	Brα				Not suff. S/N			20
	Pfα				Flat			15
β Lib	Brβ	(a)	6.6	−9.8	575	30	0.88	>150
	Brα	(a)	8.3	−24	580	5	0.90	>150
	Pfα				Flat			20

velocities in the atmosphere of τ Sco are also found to have effects in the UV (Lamers & Rogerson 1978). Also, from photospheric metal line transitions in the optical, Smith & Karp (1978) found evidence for stochastic motions in the photosphere of this star.

As mentioned, the observed spectra also show the presence of several He I lines. In some cases these lines blend with the observed H I profile and affect the shape of these profiles. The most prominent one is He I λ 4.049 situated at −240 km s^{-1} relative to Brα. It shows weak emission for the later spectral type stars: ϵ Cen, γ Peg and α Pav (and possibly ζ Dra), causing a strong asymmetry in the Brα absorption profile (see Fig. 2). Zaal et al. (1997) also found He I λ 4.049 emission for ι Her (B3IV) and θ Oph (B2IV). This suggests that it shows significant emission for stars of spectral type B1−B3. As in the case of ι Her the measured velocity of the He I λ 4.049 line is small (i.e. 5 km s^{-1} relative to the center of mass of the star), its origin is most likely photospheric. He I λ 4.049 is also suspected to be in emission for δ Cir, 10 Lac, τ Sco, and θ Car. We conclude that the line asymmetry in Brα for stars with spectral type B1−B3 can qualitatively be explained by line emission in the He I λ 4.049 line. We also suspect that the weak asymmetry in the Brβ line profile

Table 3. Identification of the strongest lines detected in at least one of the programme stars (see Figs. 1–3). The vacuum wavelength values of helium are from Martin (1987)

sp.range $\lambda_{0,\mathrm{vac}}[\mu\mathrm{m}]$	Id	Line transition	λ_{vac} [μm] ([km s^{-1}])
Brβ	a	He I 1s6f−1s4d ($S=3$)^a	26192.1 (−760)
26258.7	b	He I 1s6f−1s4d ($S=1$)^b	26205.6 (−606)
	c	He I 1s6g−1s4f (S=1,3)^c	26240.9 (−203)
	d	He I 1s5f−1s4d ($S=3$)^d	40377.3 (−1075)
Brα	e	He I 1s5f−1s4d ($S=1$)^e	40409.3 (−838)
40522.6	f	He I 1s5g−1s4f ($S=1$)^f	40490.0 (−241)
	g	He I 1s5g−1s4f ($S=1,3$)^g	40490.3 (−239)
Pfα	h	H I 8−6^h	75024.9 (+1713)
74598.6	i	H I 11−7^i	75081.1 (+1939)

of γ Peg and α Pav can be attributed to weak emission in He I 1s6g−1s4f at −203 km s^{-1} relative to Brβ. However, the blue-shifted peak-velocity of the Brβ absorption in α Pav (−65 km s^{-1}, see Fig. 1) can not be explained by this He I blend and may be related to its binary nature.

Other weak He I lines in the profiles of Brβ and Brα only show weak absorption, possibly with the exception of He I 1s5f−1s4d (at −1075 km s^{-1} relative to Brα) which may be in emission in case of τ Sco. Although it is hard to define a proper continuum in the region of Brβ, the observations indicate that the blue absorption wing of this line is more enhanced for the earliest spectral types in our sample. We attribute this asymmetry to the presence of weak He I absorption lines. For late B-type stars, such as ζ Dra and β Dra, the absorption in these He I lines is much weaker, resulting in more symmetric Brβ profiles (see Fig. 1). Within the spectral range of Pfα we could only detect the H I 8−6 and H I 11−7 line blends in the spectrum of τ Sco and α Cru. In both stars these two lines are, like Pfα, in emission.

The presence of He I absorption and/or emission can not explain all asymmetries. For the two O stars, δ Cir and 10 Lac, and for τ Sco the spectra show additional asymmetric features. In case of 10 Lac, for instance, the central reversal in Brβ is blue-shifted to −54 km s^{-1}. Also the peak velocity of Brα emission of these three stars is significantly blue-shifted. The Brα spectrum of 10 Lac and δ Cir even show additional asymmetric features. In both stars a redshifted absorption feature is present at respectively ∼+200 and +300 km s^{-1} (see Fig. 2). Zaal et al. (1997) found the same asymmetries in Brα for 10 Lac and τ Sco. In case of 10 Lac they also found blue-shifted line core emission, similar to that found here for Brβ. These

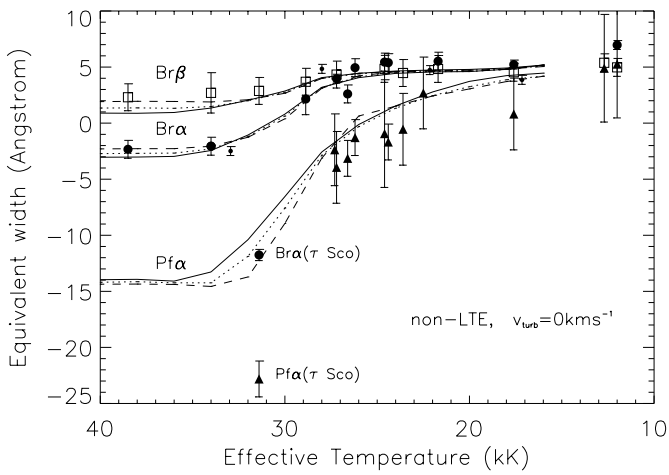

Fig. 4. The observed equivalent width of Brβ (square), Brα (circle) and Pfα (triangle) profiles versus T_{eff}. The EWs derived from non-blanketed model calculations are given for three different $\log g$ values: 4.3 (solid), 4.0 (dotted) and 3.7 (dashed). Both observed and predicted equivalent widths were measured over a wavelength of ±300 km s^{-1} relative to the rest wavelength of each line. We included also four Brα EWs (small symbol size) obtained with UKIRT (Zaal et al. 1997). The adopted effective temperatures are derived from optical analyses (references are given in Table 5)

asymmetries can not be explained by contamination of He I lines and must be intrinsic to the velocity field in the line forming region. The fact that these asymmetries occur only for stars with the earliest spectral types in our sample may suggest that the H I lines are affected by a stellar wind. However, in Paper I we demonstrated that for τ Sco the line displacements of the observed H I lines do not seem to fit to the scenario of an accelerating outflow. If these lines are affected by a stellar wind one would expect to find a correlation between depth of formation and line displacement, which is not present for τ Sco. The observed line displacements for 10 Lac point to the same conclusion. Possibly, the observed asymmetries in the H I infrared lines of these early-type stars are due to (macro) turbulent motions in the outer photospheric region.

3. The HI infrared lines as a diagnostic for T_{eff}

In this section we will demonstrate that the observed H I lines can be used as a diagnostic tool to determine stellar parameters, especially effective temperature T_{eff}. Figure 4 shows the observed EWs of the Brβ, Brα and Pfα lines plotted against T_{eff}. We have included four Brα measurements (1 Cas, HD 155889, ι Her and θ Oph) obtained from UKIRT spectra (Zaal et al. 1997) in order to improve the sampling for this line. The effective temperatures used in Fig. 4 are based on optical data. For most B-type stars the temperature is derived from Geneva photometry (Conny Aerts, private communication) following the method described by Kunzli et al. (1997). The adopted

Table 4. The predicted line strengths for Brβ, Brα and Pfα using TLUSTY (as plotted in Fig. 4). The equivalent widths were measured between a wavelength of ± 300 km s^{-1} relative to the rest wavelength of each line. For each effective temperature, three different $\log g$ values are considered: 3.7, 4.0 and 4.3, and two different values for the turbulent velocity: 0 and 25 km s^{-1}. Some high $v_{\rm turb}$ calculations at 18 000 and 20 000 K did not properly converge

$T_{\rm eff}$	$v_{\rm turb} = 0$ km s^{-1}								
	$\log g$			$\log g$			$\log g$		
	3.7	4.0	4.3	3.7	4.0	4.3	3.7	4.0	4.3
[kK]	EW(Brβ) [Å]			EW(Brα) [Å]			EW(Pfα) [Å]		
16	5.0	5.1	5.2	5.2	5.2	5.2	4.2	4.2	4.5
18	4.8	4.8	4.9	4.8	4.8	4.9	3.7	3.9	4.2
20	4.7	4.7	4.8	4.6	4.6	4.7	3.1	3.2	3.7
22	4.7	4.7	4.7	4.7	4.6	4.6	2.4	2.5	2.8
24	4.6	4.6	4.6	4.6	4.4	4.5	1.5	1.3	1.5
26	4.4	4.4	4.4	4.2	4.1	4.0	0.6	−0.3	−0.1
28	4.0	4.0	4.1	3.1	3.2	3.2	−3.1	−2.9	−2.6
30	2.7	2.8	2.9	0.4	0.8	1.1	−8.9	−7.6	−6.5
32	2.1	2.0	2.0	−1.3	−1.1	−0.7	−13.7	−11.9	−10.4
34	1.9	1.5	1.3	−2.1	−2.4	−2.4	−14.6	−14.2	−13.3
36	1.9	1.3	0.9	−2.3	−3.0	−3.3	−14.4	−14.2	−14.1
38	1.9	1.4	0.9	−2.3	−3.0	−3.5	−14.4	−14.1	−13.9
40	1.9	1.3	0.9	−2.3	−3.0	−3.5	−14.4	−14.2	−14.0
$T_{\rm eff}$	$v_{\rm turb} = 25$ km s^{-1}								
	$\log g$			$\log g$			$\log g$		
	3.7	4.0	4.3	3.7	4.0	4.3	3.7	4.0	4.3
[kK]	EW(Brβ) [Å]			EW(Brα) [Å]			EW(Pfα) [Å]		
16	4.6	4.6	3.6	4.4	4.3	4.0	2.2	1.9	7.1
18	4.3	–	–	3.6	–	–	1.3	–	–
20	–	–	4.1	–	–	3.3	–	–	0.7
22	4.1	4.0	4.0	3.3	3.2	3.2	0.2	−0.1	−0.1
24	4.0	3.9	3.9	3.2	3.0	3.0	−0.7	−1.1	−1.3
26	3.8	3.7	3.7	2.7	2.6	2.5	−3.4	−3.2	−3.0
28	3.1	3.2	3.2	0.6	1.2	1.5	−9.5	−6.9	−6.0
30	2.1	2.3	2.4	−1.8	−1.1	−0.5	−15.9	−13.1	−10.2
32	1.6	1.5	1.5	−3.5	−3.3	−2.7	−18.9	−17.1	−14.9
34	1.5	1.0	0.8	−4.2	−4.5	−4.5	−18.6	−18.2	−17.2
36	1.4	0.9	0.5	−4.4	−5.0	−5.2	−18.2	−17.7	−17.2
38	1.4	0.9	0.5	−4.3	−5.0	−5.3	−17.9	−17.5	−16.8
40	1.4	0.8	0.4	−4.1	−4.9	−5.2	−17.6	−17.4	−16.8

$T_{\rm eff}$ for δ Cir, τ Sco and θ Car result from optical line fitting of H I and/or He I (Vacca et al. 1996; Kilian 1992; Cohen et al. 1997). For 10 Lac we used the averaged literature value given by Brandt et al. (1998). The EWs are measured over a wavelength interval ranging from −300 to +300 km s^{-1} relative to rest wavelength, i.e. similar bounds as selected in Paper I. A larger bound is not preferable as it would strongly increase the error in the measured equivalent width, as this is proportional to the uncertainty in the level of the continuum multiplied by the wavelength interval over which the EW is determined.

Also shown in Fig. 4 are the hydrogen EWs predicted in Paper I based on hydrostatic H&He non-LTE model atmospheres for three different $\log g$ values: 4.3 (solid), 4.0 (dotted) and 3.7 (dashed). Table 4 provides a listing of equivalent width values plotted in Figs. 4 and 6. We will discuss these models in some detail in Sect. 4. At this point, we suffice to say that the models do not account for a turbulent velocity field.

A comparison of observed and predicted values demonstrates that the EWs agree reasonably well. One can clearly see that each individual line is temperature

Table 5. The effective temperature and $\log g$ as derived from optical photometry or spectroscopy and the three values of $T_{\rm eff}$ as derived from the equivalent widths of the individual infrared lines. The references for the optical value of $T_{\rm eff}$ and $\log g$ are: (1) the relation between $T_{\rm eff}$ and spectral class given by Vacca et al. (1996); (2) from the range of spectroscopic values (Brandt et al. 1998); (3) values derived from Geneva photometry (Conny Aerts, private communication) applying a method described by Kunzli et al. (1997); (4) Cohen et al. (1997); (5) Kilian (1992)

name	Spt.	$T_{\rm eff}$ [kK]	$\log g$	Ref.	$T_{\rm eff}$ (kK) Brβ	Brα	Pfα
β Lib	B8V	12.0 ± 0.1	3.57 ± 0.02	3	–	–	–
δ Cir	O7.5III(f)	38.5 ± 1.7	3.6 ± 0.1	1	$\gtrsim$30	$\gtrsim 32$	–
10 Lac	O9V	34 ± 4	4.1 ± 0.1	2	–	$\gtrsim 31$	–
τ Sco	B0V	31.4 ± 0.3	4.24 ± 0.03	5	30 ± 3	–	–
θ Car	B0Vp	28.9 ± 1.5	4.02 ± 0.10	4	$\lesssim 31$	28.5 ± 1	–
δ Sco	B0.3IVe	27.3 ± 0.9	4.0 ± 0.15	3	–	–	27.5 ± 2
β Cru	B0.5III	27.2 ± 1.0	3.8 ± 0.05	3	$\lesssim 29$	27 ± 2	28.5 ± 1
α Cru	B0.5IV	26.6 ± 0.6	3.85 ± 0.05	3	–	28 ± 2	28 ± 1
α Vir	B1III-IV	24.4 ± 0.5	3.90 ± 0.05	3	–	$\lesssim 20$	27 ± 2
β Cen	B1III	26.2 ± 0.7	3.80 ± 0.10	3	–	$\lesssim 26$	27 ± 2
ϵ Cen	B1III	24.6 ± 0.4	3.90 ± 0.05	3	$\lesssim 28$	$\lesssim 18$	27 ± 5
α Lup	B1.5III/Vn	22.5 ± 0.3	3.81 ± 0.04	3	–	–	$\lesssim 26$
κ Sco	B1.5III	23.6 ± 0.2	3.66 ± 0.02	3	$\lesssim 29$	–	26 ± 4
γ Peg	B2IV	21.7 ± 0.5	3.80 ± 0.06	3	$\lesssim 28$	$\lesssim 19$	–
α Pav	B2IV	17.6 ± 0.1	4.13 ± 0.02	3	$\lesssim 27$	$\lesssim 18$	–
ζ Dra	B6III	12.7 ± 3.7	3.7 ± 0.1	3	–	–	–
β Lib	B8V	12.0 ± 0.1	3.57 ± 0.02	3	–	–	–

sensitive only in a limited range. For Pfα the dependence on $T_{\rm eff}$ is strongest, showing a decrement of more than 17 Å going from 34 to 20 kK. For Brα the dependence on $T_{\rm eff}$ is also significant, showing a decrement of about 8 Å going from 34 to 26 kK. For Brβ, however, the dependence on temperature is rather weak. Note that between 17 and 27 kK the observed Pfα line strengths seem to be systematically lower than predicted by our models. We will return to this discrepancy below. In general, the sensitivity of the line strengths to gravity appears to be weak. Even when the equivalent width is determined over a larger wavelength interval, i.e. including the more gravity sensitive line wings, we found that the sensitivity to this parameter remains weak. For temperatures larger than 34 kK, the *EW*s of Brα and Brβ do show some dependence on $\log g$, although in view of the errorbars on the observed *EW*s (see Fig. 4) this sensitivity is too weak to be useful. The same holds for the *EW* of Pfα at $28 \lesssim T_{\rm eff} \lesssim 33$ kK.

We now apply the model results in Fig. 4 to derive effective temperatures from the infrared. Table 5 presents these derived temperatures and compares them with $T_{\rm eff}$ and $\log g$ values from optical analyses. In those regimes where the observed *EW* changes rapidly with temperature, the diagnostic can be used to derive fairly accurate $T_{\rm eff}$ values. The range in spectral types for which this can be done is largest for Pfα. This line may be used for spectral types between O9 and B2, i.e. for stars with temperatures between $33 \lesssim T_{\rm eff} \lesssim 20$ kK. For Brα the interval is somewhat smaller, extending from O9 to B1. The Brβ line shows the weakest dependence on temperature. The temperature interval in which it can be applied is similar to that for Brα. As a result of a rather poor continuum determination, yielding relatively large errors in equivalent width, we could only apply Brβ for the B0 V star τ Sco. The line yields upper limits for several other programme stars.

How accurate are the derived temperatures? The absolute flux level of Pfα is about a factor of 3 to 4 lower compared to the flux at the Brα wavelength. Also, the SWS sensitivity at Pfα (observed in band 2) is significantly lower compared to the sensitivity at Brα. These differences imply that the error in the line strength determination of Pfα will be much larger than the error estimate for Brα. This cancels out the larger predicted $T_{\rm eff}$ sensitivity of Pfα. In practice the reliability of both lines as a $T_{\rm eff}$ diagnostic is about equal in the range in which they both may be applied and amounts to an intrinsic error $\Delta T_{\rm eff} \sim \pm\ 1{-}2$ kK.

As noted above, a discrepancy exists between observed and predicted Pfα strength in the range $20 \lesssim T_{\rm eff} \lesssim 28$ kK (corresponding to spectral types B0.5-B2). Here the predicted *EW* is systematically higher by about 1−2 Å, which relates to an infrared temperature about 1−2 kK higher than the temperatures derived from the optical. We will return to this systematic shift in Sect. 4, where we will show that it is connected with the neglect of turbulence in the set of models shown in Fig. 4.

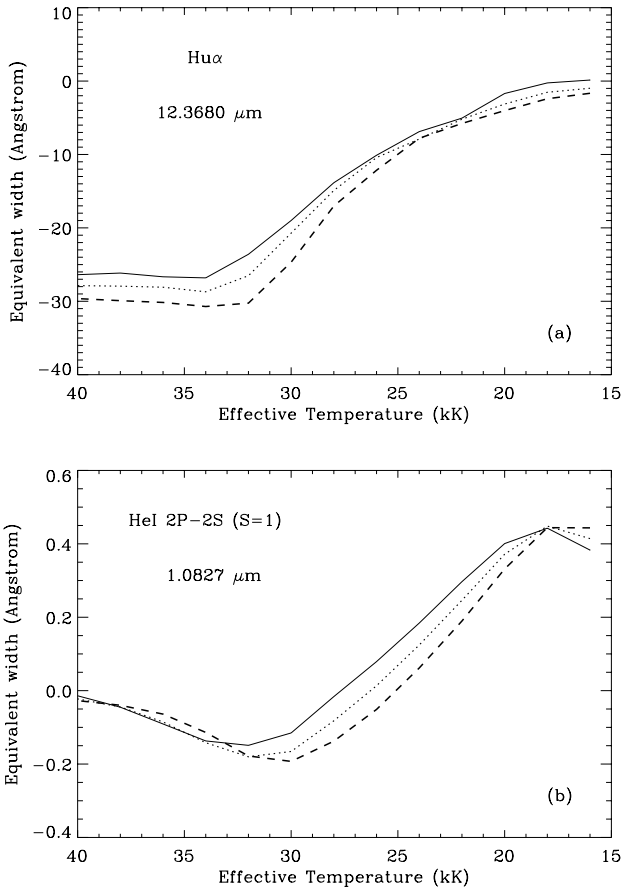

Fig. 5. The equivalent width for **a)** Huα and **b)** He I 1.083 μm as derived from the non-LTE models for three different $\log g$ values: 3.7 (dashed), 4.0 (dotted) and 4.3 (solid)

The above implies that the EW of Brα may be used directly for spectral classification. We find that the line allows for an identification to within about one subclass in the spectral range O9−B0.5. The Pfα line yields an accuracy of one to three subtypes within the range B0.5−B2. However, this last error may be narrowed down to about 1 to 1.5 subclasses when turbulence is included (see Sect. 4). The equivalent widths of Brα as obtained with [CGS4] UKIRT (Zaal et al. 1997) have errorbars about two times smaller than those obtained with SWS (see Fig. 4). If one can secure spectra of similar quality, i.e. spectra with resolution $R \gtrsim 10\,000$ and signal-to-noise $S/N > 50$, the Brα line may even be suited to derive the spectral type to within half a subclass for stars within the spectral range O9−B1.

We may also use our models to predict to what extent other infrared lines, not observable with ISO, may be used as a temperature diagnostic. First we discuss Huα at 12.4 μm. This particular line may be observed using VISIR (VLT Image and Spectrometer for mid InfraRed), scheduled to be installed in 2001 on the Very Large Telescope (VLT). With this instrument it should be possible to obtain Huα spectra with sufficient S/N for most of our program stars. Figure 5a shows the predicted EW of this line as a function of temperature. Compared to Pfα, Huα shows an even larger sensitivity to $T_{\rm eff}$ extending down to temperatures as low as ∼17 kK (spectral type B3). We conclude that this line is expected to be an excellent infrared $T_{\rm eff}$ diagnostic for O9 to B3 type stars. Next, we investigate to what extent He I infrared lines may be used as temperature diagnostics. Figure 5b shows the equivalent width behaviour for He I 1.083 μm. The gravity sensitivity of this line is like that of the hydrogen lines rather weak. Unfortunately also the $T_{\rm eff}$ dependence of this He I line is weak, rendering the line almost useless for $T_{\rm eff}$ determination unless very high quality spectra can be secured ($S/N \gtrsim 1000$). A second prominent He I line in the infrared is He I λ 2.058. The strength of this line is, however, strongly coupled to the strength of the UV continuum through the resonance transition at 584 Å (Morris et al. 1996). This makes this line unsuited for spectral classification. We conclude that helium infrared lines are not expected to yield a sensitive temperature calibration method for stars of spectral type O9−B3, unless very high S/N data is available for He I 1.083 μm.

4. The validity of the hydrostatic H&He model

The predicted equivalent widths discussed in the previous section are based on non-LTE hydrostatic H&He model calculations. In this section we will test to what extent some of the assumptions in these models will affect the temperature determination. First, we will compare the observed line strengths with LTE calculations to demonstrate that non-LTE is a crucial physical ingredient for modeling the observed EWs. Secondly, we will show that when accounting for line blanketing, one does not expect to affect the predicted line strength significantly. Thirdly, we describe the effect of turbulence. By including a turbulent velocity of 15 km s^{-1} in the model calculations we are able to explain the mismatch between the observed Pfα EW and those predicted. Finally, we will discuss whether a stellar wind may be expected to have an effect on the H I and He I infrared lines.

4.1. Equivalent width predictions from LTE models

Figure 6a shows the observed EWs together with model predictions from LTE calculations. Only one gravity ($\log g = 4.0$) was used. The predicted values for Pfα are strikingly different from the non-LTE results for all of the investigated $T_{\rm eff}$ range. Large discrepancies also occur for Brα at $T_{\rm eff} \gtrsim 26$ kK. At $T_{\rm eff} \lesssim 26$ kK the LTE assumption seems to be reasonable for both Brα and Brβ. However, close inspection of the predicted profiles indicates that at these temperatures non-LTE effects are also important. The agreement between the LTE and non-LTE models at $T_{\rm eff} \lesssim 26$ kK is merely coincidental: in the case of LTE the line center is deeper, whereas the line wings are weaker compared to the non-LTE profiles. These differences happen to cancel out approximately, yielding the same value for the equivalent width. In general we conclude that LTE

calculations fail to predict the strengths and shapes of the investigated infrared hydrogen lines for stars with spectral type earlier than B3. The same conclusion is reached for the strongest infrared neutral helium lines.

4.2. The effect of line blanketing

The term "line blanketing" signifies the effect that millions of spectral lines may have on the structure of a stellar atmosphere. In Paper I, we demonstrated that for τ Sco a model accounting for line blanketing in general yielded better infrared hydrogen profile fits. Typically, the profiles show a slightly enhanced core emission and a moderately enhanced wing absorption compared to H&He predictions. Essentially, these effects are a direct result of differences in the temperature structure, the temperature gradient in the line blanketed models being somewhat steeper. In τ Sco the differences in line shape are most pronounced for Brβ and Brα. Compared to the non-blanketed case the equivalent width of Brβ is increased by about 1 Å (i.e. overall stronger line absorption). An effect of this magnitude may explain the systematic offset between observed and predicted strength of this line at $T_{\rm eff} \gtrsim 31$ kK, but should not occur at lower temperatures when the line fits the non-blanketed models used in Fig. 4 well. The *overall* strength of Brα and Pfα was not found to be much different between the blanketed and non-blanketed case.

Although one should not blindly extrapolate the results for τ Sco to the entire temperature regime investigated in this paper, the test case does seem to indicate that the effect of blanketing on the equivalent width is relatively modest. This also seems to be validated by the success of the H&He models in reproducing the observed infrared line strengths. To some extent this may be explained by the fact that the *EW* is calculated using bounds of ± 300 km s^{-1}. For this interval the "extra" absorption in the wings of lines of models incorporating blanketing about cancels the "extra" emission in the line center.

Unfortunately, it is not easy to extend our blanketing calculations such that they cover the temperature range of all late-O and early-B stars. The computational costs of such a grid are presently too large.

4.3. The effect of turbulence

In the models the effects of turbulence have been neglected. Turbulence is expected to enhance non-LTE effects in the strongest IR hydrogen and helium lines. The presence of strong turbulence is likely the reason why the observations of τ Sco differ from our model predictions (see Paper I). To illustrate this: in τ Sco a broad emission is seen in Brα reaching velocities of ± 150 km s^{-1}.

Figure 6b shows models similar to those given in Fig. 4, now using a $v_{\rm turb}$ of 25 km s^{-1}. Table 4 provides a listing of equivalent width values plotted in Fig. 6. For all temperatures we find that the *EW* of Brα and Pfα decrease

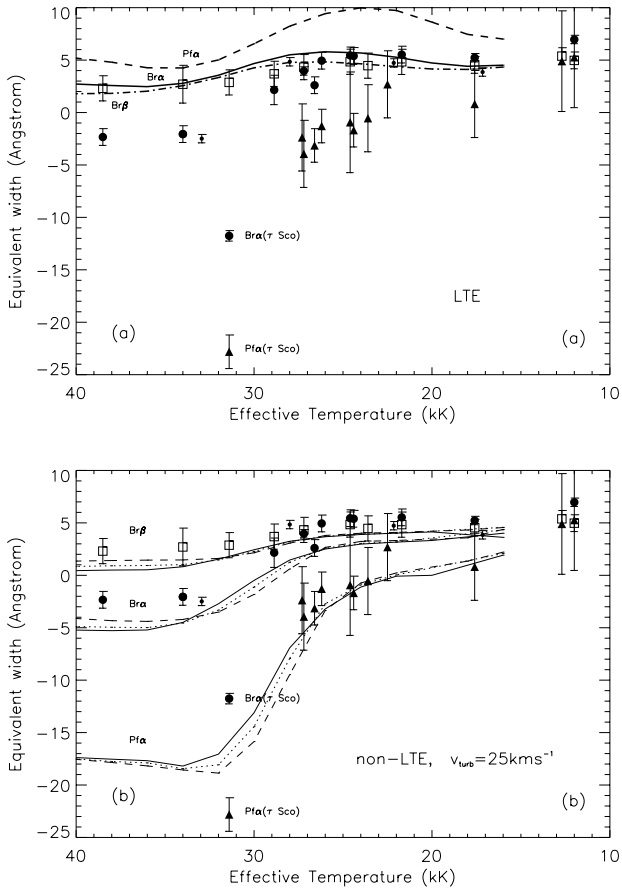

Fig. 6. a) Comparison between observed equivalent widths for Brα (solid), Brβ (dot-dashed) and Pfα (dashed) and predicted values assuming LTE and $v_{\rm turb} = 0$ km s^{-1}, and **b)** assuming non-LTE and $v_{\rm turb} = 25$ km s^{-1}. For the LTE models we only used $\log g = 4.0$. In the case of non-LTE models the same gravity values (and linestyles) are used as in Fig. 4

(i.e. stronger line emission) by respectively ∼2 and 3.5 Å. The introduction of $v_{\rm turb}$ will make the overall fit worse for Brβ and Brα, whereas for Pfα a $v_{\rm turb}$ of ≈ 15 km s^{-1} will remove the overall discrepancy between observed and predicted equivalent width using H&He models. For the observed Pfα lines which show line emission, i.e. those with spectral type B0.5−B2, the line is expected to be purely photospheric as possible wind contamination can likely be ruled out for such spectral types (see Sect. 2.1). As the overall line formation of Pfα occurs further out in the photosphere compared to Brα, this may indicate that $v_{\rm turb}$ increases outward in the atmosphere of dwarfs of spectral type B0.5−B2. A detailed quantification of the turbulent velocity gradient requires a detailed analysis of line contribution functions, based on models with much higher spatial resolution than the ones used in this study (which have 50 radial depth points). This is beyond the scope of the present paper. In any case, this interesting result demonstrates the potential of H I infrared lines in studying the outer photospheric structure of early-type stars.

4.4. The effects of a stellar wind

We will now address the possible presence of a stellar wind and its effect on the infrared profiles. The H&He model calculations assume a hydrostatic atmosphere. In Paper I we have demonstrated that in case of τ Sco a wind is not expected to affect the H I and He I line profiles. This conclusion is based on both an observational and a theoretical argument.

First, the observed line displacements for the different hydrogen lines do not seem to correlate with the rest wavelengths ($\lambda_\circ$'s) of these lines in the sense that a larger displacement is expected for lines with larger $\lambda_\circ$. This is expected as due to the λ^2 proportionality of free-free processes, the infrared continuum forming layers shift outward in the atmosphere. If a measurable velocity gradient would already be present in these layers a larger displacement should have been seen in, for instance, Pfα compared to Brα. Second, after linking the density structure to a velocity structure using the mass continuity equation, inspection of the τ Sco model showed that the cores of the lines discussed in this study all formed in highly subsonic layers.

We expect these arguments also to apply to the low mass-loss rates of the B-type dwarfs and (sub)giants investigated in this paper. (For B-supergiants the argument no longer holds as these stars suffer a much larger mass loss. See e.g. Najarro et al. 1998). As discussed in Sect. 5.2.1, the earliest spectral types in our sample show evidence for asymmetries in the observed hydrogen profiles which could not be attributed to He I blends. We can not fully exclude that these asymmetries are the result of a stellar wind, however, at the present moment it seems more reasonable to attribute them to macro turbulent velocities in the outer photosphere, as already suggested for τ Sco (Paper I).

5. Discussion

Earlier work discussing infrared spectroscopy for spectral classification of OB stars was published by Hanson et al. (1996, 1998) and Blum et al. (1997). These groups focus on the classification of supergiants, although their samples also include some (sub)dwarfs.

Hanson et al. (1996) used Brγ, He I λ 2.058, 2.116, He II λ 2.190 and some metal line transitions in the K-band (2.04−2.2 μm) for the classification of 180 optically visible, luminous OB stars. For the late O- and B-type dwarfs they could derive only a coarse classification as only Brγ and He I λ 2.116 could be used. In Sect. 3 we have demonstrated that Brβ is not ideal for spectral classification. As the spectral dependence for Brγ is even weaker (see Paper I), this explains why Hanson et al. (1996) are only able to provide a coarse spectral classification, with "coarse" meaning the stars may be grouped in "early", "mid" and "late" type. First attempts using the H-band for spectral classification (Blum et al. 1997; Hanson et al. 1998) yield similar results. Hanson et al. (1998) examined the spectral characteristics of 34 normal OB stars using the He I λ 1.700, He II λ 1.693 and the Br 11 1.7681 μm lines in the H-band. For late O- and B-type dwarfs again only a coarse spectral classification could be derived. Compared to the K-band it is also more difficult to find a luminosity effect in these lines, although Hanson et al. (1998) appear to reveal a weak luminosity dependence using the ratio of Br 11 to He I 1.700 μm.

In comparison with these spectral classifications using the K- and H-band, spectral classification using the Brα and Pfα line appears much more promising as these lines show a significantly stronger dependence on stellar temperature for the late O- and early B-type dwarfs allowing for a classification within one or two subclasses. The accuracy of the spectral classification is expected to improve when Huα becomes observable with the installation of VISIR in 2001 on the VLT. Contamination by excess flux at longer wavelengths ($\lambda \gtrsim 4$ μm) due to warm circumstellar dust is not anticipated to be an important problem, as dust is not expected to be present in dwarfs or subgiants. However, dust contamination is expected for supergiants. Therefore, the use of Pfα or Huα for spectral classification of supergiants may not be feasible, unless the dust contamination is weak or can be modeled.

With the observed line profiles we were not able to put constraints on the value of $\log g$. Gravity causes only minor changes in the derived equivalent widths for the observed H I infrared lines. As one also has to deal with the uncertainty in microturbulent velocity, we expect it to be difficult to determine $\log g$ using the EW of H I and/or He I lines. Alternatively one could derive the gravity by fitting the Stark broadened wings of hydrogen lines like, Brβ and Brγ. However, this requires high quality spectra with well determined continua and also a more complex modeling accounting for the effects of line blanketing.

The K-band atlas of Hanson et al. (1996) includes the He I λ 2.058 line. These data allows for a comparison of observed and predicted equivalent widths. Figure 7 shows this comparison for the normal stars in their sample, i.e. excluding the emission line stars. In order to link the spectral type adopted by Hanson et al. (1996) to a temperature value we used the spectral class calibrations given by Vacca et al. (1996) for the O-type stars and those from Meyer et al. (1998) for the B-type stars. To allow for a comparison of the more evolved stars, we extended our gravity calculations to include $\log g = 3.4$ and 3.0.

Figure 7 shows that for the O-type stars the predicted equivalent widths are in fair agreement with the observations. The supergiants (large dots) show the largest equivalent widths, whereas the main sequence stars (small dots) have an $|EW| \lesssim 0.5$. The observed equivalent widths of the supergiants may be reproduced when including low gravity models. Note however that also an increase in the microturbulent velocity (the dashed lines are for $v_{\rm turb}$= 25 km s^{-1}) helps bring the models in range of these observations. The large scatter in the observed EWs for the O supergiants indicates that the correlation between He I λ 2.058 strength and luminosity is not pronounced. In the case of the B1-B2 supergiants the observed He I

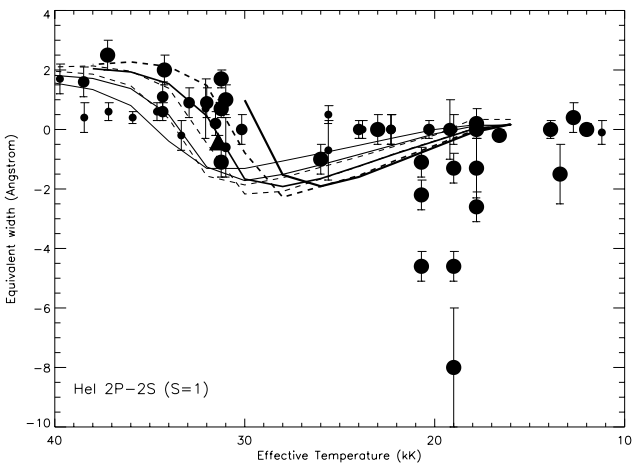

Fig. 7. Comparison between the equivalent width of the observed He I 2.058 μm line as given by Hanson et al. (1996) and those predicted in Paper I. The observed EWs are represented by dots. The large (medium, small) dots represent supergiants (giants, dwarfs). The model calculations are shown for four different values of $\log g$: 4.3, 3.85, 3.4 and 3.0 (increasing line thickness). The dashed lines represent similar model calculations using a $v_{\rm turb}$ of 25 km s^{-1}; these calculations have not been performed for the lowest gravity value

strength also shows a large scatter. For these later type supergiants the hydrostatic H&He models completely fail to predict the observed strong He I λ 2.058 line emission. The reason for this large discrepancy is most likely due to the presence of a strong stellar wind.

However, one should be very prudent in applying this line. The resonance 1s2p–1s1s transition at 584 Å shares the same upper level with the He I λ 2.058 transition. The population of this upper level is dominated through the resonance channel. This implies that the He I λ 2.058 line is strongly sensitive to variations of the flux in the far-UV part of the spectrum (Morris et al. 1996). The line will thus respond to even minor density enhancements near the surface of the star. Such density variations are expected to be present in the onset of the stellar wind of early-type stars (Owocki et al. 1988). This may render He I λ 2.058 unsuited for spectral classification, especially for the more luminous supergiants. For the dwarfs the He I λ 2.058 line is weak. In Paper I, we observed the He I λ 2.058 profile of τ Sco which showed a weak red-shifted line emission. The line shape nor strength could be explained using a hydrostatic model. This serves to demonstrate the complexity of the He I λ 2.058 line formation, not only in supergiants but also in case of dwarfs.

6. Summary

We have demonstrated the potential of determining the stellar temperature from the equivalent width of Pfα and Brα. These lines are sensitive to temperature for dwarfs and giants within the spectral range O9−B2 (O9−B1 in case of Brα). The Brα sensitivity to $T_{\rm eff}$ is less strong compared to Pfα. The quality of our observations allow one to derive a spectral type within $\sim$ one or two subclasses. Using high resolution and high S/N spectra obtained with UKIRT, the classification may be improved to within one subclass, using Brα. The EW of Brβ depends only weakly on $T_{\rm eff}$ over the entire investigated spectral range. Therefore this line as well as higher Brackett series lines have only very limited potential for spectral classification.

Compared to the optical spectral classification, the effective temperatures estimated from Brα and Pfα lines have errorbars about a factor of two to four larger. As the $\log g$ dependence is weak for the observed infrared lines, we presently need to rely on the optical for a determination of the luminosity class. In the future one may be able to determine gravity from fitting Stark broadened lines like Brβ and Brγ. However, this requires high quality spectra with well determined continua and also a more realistic modeling, accounting for line blanketing.

The Brβ, Brα and Pfα line strengths as determined from models (Paper I) show a promising agreement with the programme stars observed with ISO. This indicates that the hydrostatic non-LTE H&He models are valid and allow for a meaningful prediction of temperature based on the H I and He I line strengths. This may seem surprising as these models are rather basic, i.e. they neglect line blanketing and/or effects of a wind. The most important ingredient in the model is to consider departures from LTE, as such departures strongly influence the equivalent width as well as the line shape.

Line blanketing seems only modestly important in determining the strengths of these infrared lines. This may in part be due to the adopted line bounds of $\pm$300 km s^{-1} used to measure the equivalent width. These bounds are such that they result in a cancelation of additional wind absorption – compared to non-blanketed predictions – by additional core emission.

Microturbulence competes in importance with line blanketing when discussing line strengths. The inclusion of these small scale motions leads to an increased line emission. Essentially, turbulence tends to desaturate the lines and may enhance non-LTE effects (Sigut & Lester 1996). In order to obtain a better overall fit between observed and predicted Pfα strength we needed to include turbulent velocities of magnitude $v_{\rm turb} \sim 15$ km s^{-1}. For Brα an optimal fit was found for $v_{\rm turb} < 5$ km s^{-1}. This points to a gradient in the turbulent velocity in the photospheres of late-O and early-B dwarfs and subgiants, in the sense that $v_{\rm turb}$ increases with decreasing density.

In comparison with the lines observed in the H- and K-band spectroscopy (Hanson et al. 1996, 1998), Brα and Pfα show a larger sensitivity to effective temperature for late O- and early B-type dwarfs. The accuracy of the spectral classification is expected to improve when using the equivalent width of Huα. This line may be observed with VISIR when installed in 2001 on the VLT.

Acknowledgements. We thank Conny Aerts (KUL, Leuven, Belgium) for providing the effective temperature of the B-type stars. The data presented was analysed with the support of the Dutch ISO Data Analysis Centre (DIDAC) at the Space Research Organization Netherlands (SRON) in Groningen. This work was supported by NWO "Pionier" grant 600-78-333 and by Spinoza grant 08-0 to E. P. J. van den Heuvel.

References

Blum, R. D., Ramond, T. M., & Conti, P. S. 1997, AJ, 113, 1855
Brandt, J. C., Heap, S. R., Beaver, E. A., et al. 1998, AJ, 116, 941
Cohen, D. H., Cassinelli, J. P., & MacFarlane, J. J. 1997, ApJ, 487, 867
Coté, J., & van Kerkwijk, M. H. 1993, A&A, 274, 870
de Graauw, T., Haser, L. N., Beintema, D. A., et al. 1996, A&A, 315, L49
Hanson, M. M., Conti, P. S., & Rieke, M. J. 1996, ApJS, 107, 281
Hanson, M. M., Rieke, M. J., & Luhman, K. L. 1998, AJ, 116, 1915
Hoffleit, D., & Jaschek, C. 1982, BSC, 4th revised ed., Yale Univ. Obs. New Haven CT
Hoffleit, D., Saladyga, M., & Wlasuk, P. 1983, A Supplement to BSC, Yale Univ. Obs., New Haven CT
Kessler, M. F., Steinz, J. A., Anderegg, M. E., et al. 1996, A&A, 315, L27
Kilian, J. 1992, A&A, 262, 171
Kunzli, M., North, P., Kurucz, R. L., & Nicolet, B. 1997, A&AS, 122, 51
Lahuis, F., Wieprecht, E., Bauer, O. H., et al. 1998, ISO-SWS data analysis, SP Conf. Ser., 145
Lamers, H. J. G. L. M., & Rogerson, J. B. Jr. 1978, A&A, 66, 417
Martin, W. C. 1987, Phys. Rev. A, 36, 3575
Meyer, M. R., Edwards, S., Hinkle, K. H., & Strom, S. E. 1998, ApJ, 508, 397
Morris, P. W., Eenens, P. R. J., Hanson, M. M., et al. 1996, ApJ, 470, 597
Murdoch, K. A., Drew, J. E., & Anderson, L. S. 1994, A&A, 284, L27
Najarro, F., Kudritzki, R.-P., Hillier, D. J., et al. 1998, in ISO's view on stellar evolution, Noordwijkerhout, The Nederlands, 1-4 July 97, ed. L. B. F. M. Waters, C. Waelkens, K. A. van der Hucht, & P. A. Zaal (Kluwer), 137
Owocki, S. P., Castor, J. I., & Rybicki, G. B. 1988, ApJ, 335, 914
Sigut, T. A. A., & Lester, J. B. 1996, ApJ, 461, 972
Smith, M. A. 1978, ApJ, 224, 927
Smith, M. A. 1985, ApJ, 297, 206
Smith, M. A., & Karp, A. H. 1978, ApJ, 219, 522
Vacca, W. D., Garmany, C. D., & Shull, J. M. 1996, ApJ, 460, 914
Valentijn, E. A., & Thi, W. F. 2000, ISO's Short Wavelength Spectrometer – Ultimate sensitivity. Reducing the effects of cosmic weather, Exper. Astron., 10, 215
Walborn, N. R. 1972, AJ, 77, 312
Walborn, N. R. 1973, AJ, 78, 1067
Zaal, P. A., Waters, L. B. F. M., Geballe, T., & Marlborough, J. M. 1997, A&A, 326, 237
Zaal, P. A., de Koter, A., Waters, L. B. F. M., et al. 1999, A&A, 349, 573, Paper I